crystals

MDPI

Article

Synthesis, Crystal Structure, and Properties of a New Coordination Polymer Built from N/O-Donor Mixed Ligands

Mei-An Zhu, Shuai-Shuai Han, Feng Deng, Jia-Le Li and Shui-Sheng Chen *

College of Chemistry & Chemical Engineering, Fuyang Normal University, Fuyang 236041, China; zhumeian2017@163.com (M.-A.Z.); shuisheng20011@tom.com (S.-S.H.); fengdengfd@yeah.net (F.D.); lijialeljl@163.com (J.-L.L.)

* Correspondence: sscfync@163.com; Tel.: +86-558-2595836

Received: 31 August 2018; Accepted: 18 September 2018; Published: 21 September 2018

Abstract: The coordination polymer, namely, $[Cd(H_2L)(nobda)]_n$ (**1**) was prepared by the reaction of $Cd(NO_3)_2{\cdot}4H_2O$ with 4-amino-1,2-benzenedicarboxylic acid (H_2nobda) and 1,4-di(1*H*-imidazol-4-yl)benzene (H_2L), and characterized by single-crystal X-ray diffraction, elemental analysis, infrared (IR) spectroscopy, thermogravimetric analysis, and powder X-ray diffraction (PXRD). The carboxylic acid of H_2nobda ligands was completely deprotonated to be $nobda^{2-}$ anions, which act as tridentate ligand to connect the Cd^{2+} to form two-dimensional (2D) network, while the neutral H_2L ligands serve as a linear didentate bridge to connect two adjacent Cd^{2+} ions upper and down the 2D layer. The adjacent 2D layers were further linked into the three-dimensional (3D) supramolecular polymer by the weak interactions such as hydrogen bonds and $\pi-\pi$ stacking interactions. The ultraviolet-visible (UV-vis) absorption spectra and luminescent properties in the solid state at room temperature have been investigated.

Keywords: coordination polymer; structural characterization; luminescent property

1. Introduction

In the past decades, the crystalline material of coordination polymers (CPs) has become an expanding research topic, not only due to their fascinating architectures and captivating topologies [1–3], but also for their potent applications in the fields of luminescence [4], gas adsorption/separation [5], chemical sensors [6], heterogeneous catalysis [7], and so on. Because the coordination polymers are composed of the metal ion and organic ligands, that is, the nature of metal ion and organic ligands are most important factors for constructing targeted CPs with desired properties [8–10]. Especially, the design of organic ligands is the key factor to build CPs. O-donor carboxylic acids are extensively employed to build diverse CPs, due to their versatile coordination modes. For example, the Yaghi group has designed a series of carboxylic acid with expanded and variously functionalized organic linkers, and has made a prominent contribution for the construction of porous CPs by reticular synthesis based on metal paddle-wheel building or infinite metal-carboxylate secondary building units (SBUs) [11,12]. Significantly, the surface area of CPs have great values ranging from 1000 to 10,000 m^2/g, which have exceeded those of traditional porous materials, such as carbons and zeolites [11]. Moreover, CPs with functional modifications exhibit favorable gas adsorption, which are typically selective gas adsorption properties for CO_2 or alkanes, and they can potentially alleviate the greenhouse effect or be employed as carriers to store energy gas [13,14]. Meanwhile, polyazaheteroaromatic ligands, another series of N-donor ligands, including the imidazole, trizole and tetrazole, are also successfully used to construct coordination

polymers [15–17]. In our previous work, we have designed 4-imidazoly-containing ligands such as 1,3,5-tri(1*H*-imidazol-4-yl)benzene and,1,4-di(1*H*-imidazol-4-yl)benzene, and we use them to assemble porous metal–imidzolate complexes that show excellent gas adsorption or selective adsorption for CO_2 gas [18,19]. Moreover, the polycarboxylates and N-donors ligands have different coordination preferences owing to the N and O atoms possessing different electron configurations. Due to their favorable compatibility for mixed polycarboxylates and N-donors ligands, we have synthesized a number of CPs with diverse structures by the reaction of mixed 4-imidazolyl and different carboxylate ligands, together with varied metal salts [20–22]. Taking the favorable adjustability for the mixed 4-imidazolyl and carboxylate ligands, we have chosen 1,4-di(1*H*-imidazol-4-yl)benzene (H_2L) and 4-amino-1,2-benzenedicarboxylic acid (H_2nobda) as mixed ligand, to react with $Cd(NO_3)_2{\cdot}4H_2O$, and we have obtained a new Cd(II) coordination polymer $[Cd(H_2L)(nobda)]_n$ (**1**) as an extension of our previous work. The UV-vis absorption spectra and luminescent properties in the solid state at room temperature have been investigated.

2. Experimental Section

2.1. Materials and Instrumentation

All the reagents were of reagent grade in this experiment. IR spectra were carried out on a Bruker Vector 22 FT-IR spectrophotometer (Bruker, Billerica, MA, USA) using KBr pellets. Elemental analyses were analyzed on a Perkin-Elmer 240C Elemental Analyzer (Perkin-Elmer, Waltham, MA, USA). Power X-ray diffraction (PXRD) patterns were performed on a Shimadzu XRD-6000 X-ray diffractometer (Shimadzu, Kyoto, Japan) with Cu$K\alpha$ (λ = 1.5418 Å) radiation at room temperature. Thermogravimetric analyses (TGA) were carried on a simultaneous SDT 2960 thermal analyzer (Thermal Analysis Instrument Inc., New Castle, DE, USA). Photoluminescence spectra for the solid samples were recorded with a HORIBA FluoroMax-4 fluorescence spectrophotometer (Horiba, Kyoto, Japan) at room temperature. FLS920P fluorescence spectrometer (Edinburgh Instruments, Edinburgh, UK) was adopted to measure the decay lifetimes.

2.2. Synthesis of $[Cd(H_2L)(nobda)]_n$ (**1**)

A reaction mixture of H_2L (0.021 g, 0.1 mmol), H_2nobda (0.0181 g, 0.1 mmol), $Cd(NO_3)_2{\cdot}4H_2O$ (0.0308 g, 0.1 mmol) and NaOH (0.008 g, 0.2 mmol) in 15 mL H_2O was sealed in a 25 mL Teflon-lined stainless steel container, and heated at 120 °C for 48 h. Colorless block crystals of **1** were collected with a yield of 62%. Analytically calculated (%) for $C_{20}H_{15}CdN_5O_4$: C, 47.87; H, 3.01; N, 13.96. Found (%): C, 47.56; H, 2.92; N, 14.11. IR(KBr): 3341−2535(m), 1602(vs), 1549(vs), 1508(m), 1388(vs), 1302(m), 1186(m), 1168(m), 1131(s), 1061(w), 956(m), 862(s), 830(m), 790(s), 702(m), 653(m), 508(m) cm^{-1}.

2.3. Crystal Structure Determination

The single crystal data of $[Cd(H_2L)(nobda)]_n$ (**1**) was collected on a Bruker Smart APEX CCD diffractometer (Bruker, Billerica, MA, USA) The structure was solved by a direct method, and refined by full-matrix least squares on F^2 using the SHELX-97 program [23]. The crystallographic data is listed in Table 1.

Table 1. Crystallographic data and structure refinement for **1**.

Empirical Formula	$C_{20}H_{15}CdN_5O_4$
Formula weight	501.77
Temperature/K	296(2)
Crystal system	Monoclinic
Space group	*C*2/c
a/Å	19.587(5)
b/Å	13.514(3)
c/Å	15.459(4)
α/°	90
β/°	118.297(3)
γ/°	90
Volume/Å^3	3602.8(16)
Z	8
ρ_{calc}mg/mm^3	1.850
μ/mm^{-1}	1.254
S	1.008
F(000)	2000
Index ranges	$-24 \leq h \leq 24$, $-16 \leq k \leq 16$, $-19 \leq l \leq 19$
Reflections collected	13368
Independent reflections	3731
Data/restraints/parameters	3731/0/271
Goodness-of-fit on F^2	1.008
Final *R* indexes [I $\geq 2\sigma(I)$]	R_1 = 0.0393, wR_2 = 0.1165
Final *R* indexes [all data]	R_1 = 0.0583, wR_2 = 0.1342
Largest diff. peak/hole/e Å^{-3}	0.938/−0.685

Crystallographic data for the structure has been deposited with the Cambridge Crystallographic Data Centre No. CCDC 1864626 for **1**.

3. Results and Discussion

3.1. Structural Description of [Cd(H$_2$L)(nobda)]$_n$ (**1**)

The result of X-ray diffraction analysis revealed that [Cd(H$_2$L)(nobda)]$_n$ (**1**) crystallizes in monoclinic *C*2/c space group. The asymmetric unit of **1** consists of one crystallographically independent Cd(II) atom, one H$_2$L ligand, and one completely deprotonated nobda^{2-}. As shown in Figure 1, the Cd1 had a distorted octahedral coordination geometry with N_3O_3 binding set, in which the equatorial plane contains N4B and O3A from two distinct H$_2$L and nobda^{2-} ligands respectively, and a pair of O1, O2 atoms from one chelating carboxylate group of nobda^{2-} ligand. The atoms N1 and N5C from two distinct H$_2$L ligands occupy the axial positions with an N1–Cd1–N5C angle of 159.79(15)° (Table 2). The Cd–N distances are 2.264(4), 2.274(4), and 2.443(4) Å while the Cd–O distance is 2.340(3), 2.364(3), 2.424(4) Å, and the coordination angles around Cd(1) are in the range of 54.72(12)°~159.79(15)° (Table 2). In this complex, two carboxyl groups from nobda^{2-} adopt μ_1-η^1:η^1-chelating and μ_1-η^1:η^0-monodentate coordination modes to coordinate with two Cd(II) atoms, while the amino from nobda^{2-} ligand also participate in coordination with another Cd(II) atom in this context; each nobda^{2-} ligand acts as a μ_3-bridge to link the three Cd(II) atoms. Two such carboxylate groups from different nobda^{2-} ligands bridge two Cd(II) atoms to give a binuclear [$Cd_2(COO)_2$] motif, with a Cd···Cd distance of 6.14 Å. Each $Cd_2(COO)_2$ binuclear unit acts as a 4-connected node to link other four identical motifs without considering the connection from H$_2$L ligands. In this connection mode, the Cd(II) atoms are linked by nobda^{2-} ligands to form a two-dimensional (2D) Cd(II)(nobda)$^{2-}$ layer structure with (4, 4) topology (Figure 2), where the [$Cd_2(COO)_2$] motif is considered as a 4-connected node. The linear H$_2$L ligands employ two-connector linkers to connect adjacent Cd(II) atoms of the same 2D layer, forming the Cd(II)(H$_2$L)(nobda)$^{2-}$ layer structure (Figure 3), which

expands the 4-connected node of $[Cd_2(COO)_2]$ motif into a 6-connected node (Figure 4). According to the simplification principle, the resulting 2D layer structure of 1 can be considered as a uninodal 6-connected net with a Schläfli symbol $(3^3{\cdot}4^{10}{\cdot}5{\cdot}6)$ by taking the $Cd_2(COO)_2$ binuclear motifs as network nodes and the H_2L and $nobda^{2-}$ ligands as 2-connected linkers (Figure 4) [24]. Particularly, the carboxyl group can easily act as a hydrogen bonding acceptor, while the NH or N atom of the imidazolyl groups act as hydrogen bonding donors, and their interaction can easily benefit the construction of coordination polymers. As a result, the structure built from the mixed ligands exists rich hydrogen bonding interaction, and the C−H···O and N−H···O (C(12)···O(2) 3.406(7) Å, C(12)–H(12)···O(2) 166°; N(3)···O(3) 2.806(6) Å, N(3)–H(3)···O(3) 142°; N(2)···O(4) 2.816(6) Å, N(2)–H(2A)···O(4) 169°) hydrogen bond exist between the 2D layers (Table 3). In addition to the hydrogen bond interaction, the π−π weak stacking interactions also exist between neighboring 2D structures. It could be found that the imidazole rings of H_2L ligands from the neighboring 2D layers are parallel, showing the π−π stacking interactions with the centroid−centroid distance of 3.57 Å [25]. In this context, the weak interactions including the π−π stacking and hydrogen bonding interactions extend 2D structure into a three-dimensional (3D) coordination polymer (Figure 5).

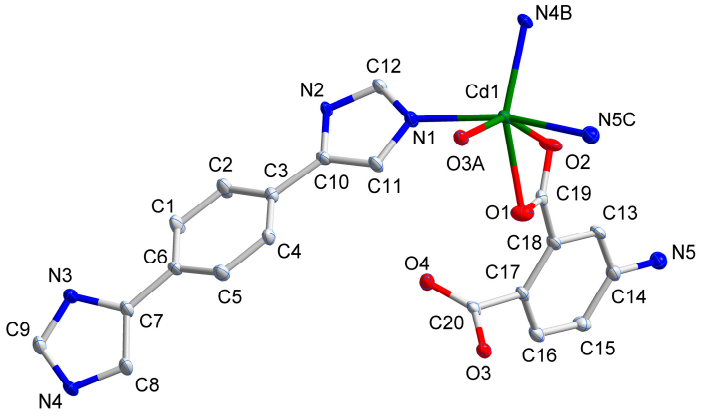

Figure 1. The coordination environment of Cd(II) ion in **1**. Symmetry code: A 0.5 − x, 0.5 − y, − z, B x, 1 + y, z, C x, 1 − y, −0.5 + z.

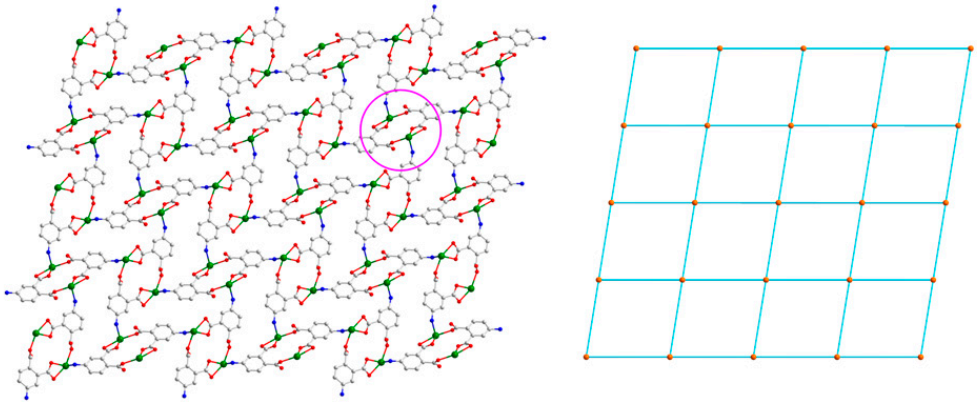

Figure 2. A 2D layer structure built from the Cd(II)$(nobda)^{2-}$ (**left**) in **1** and schematic representation of 2D network with (4, 4) topology (**right**).

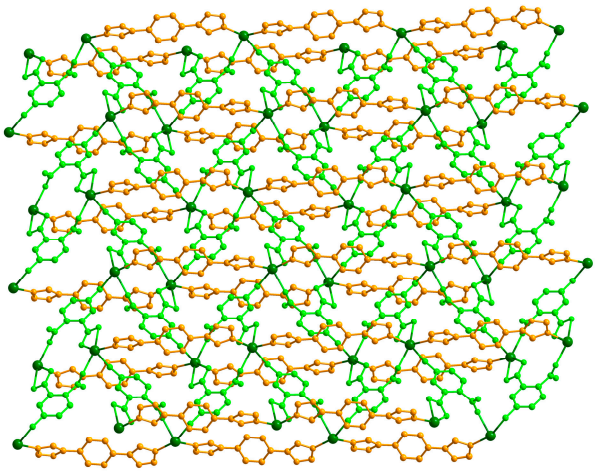

Figure 3. 2D framework of Cd(II)(H_2L)(nobda)$^{2-}$ in **1**.

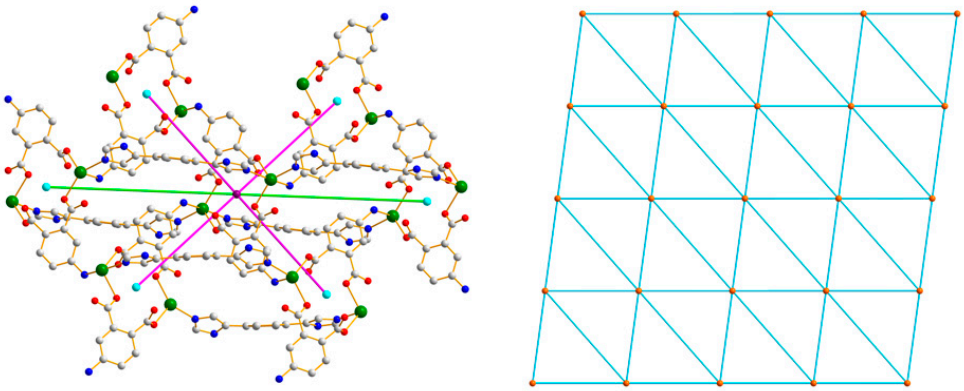

Figure 4. The 6-connected node based on the binuclear unit in **1** linked by the nobda^{2-} and H_2L ligands (**left**); A view of the uninodal 6-connected net with the Schläfli symbol ($3^3 \cdot 4^{10} \cdot 5 \cdot 6$) in complex **1** based on $Cd_2(COO)_2$ binuclear motifs (**right**).

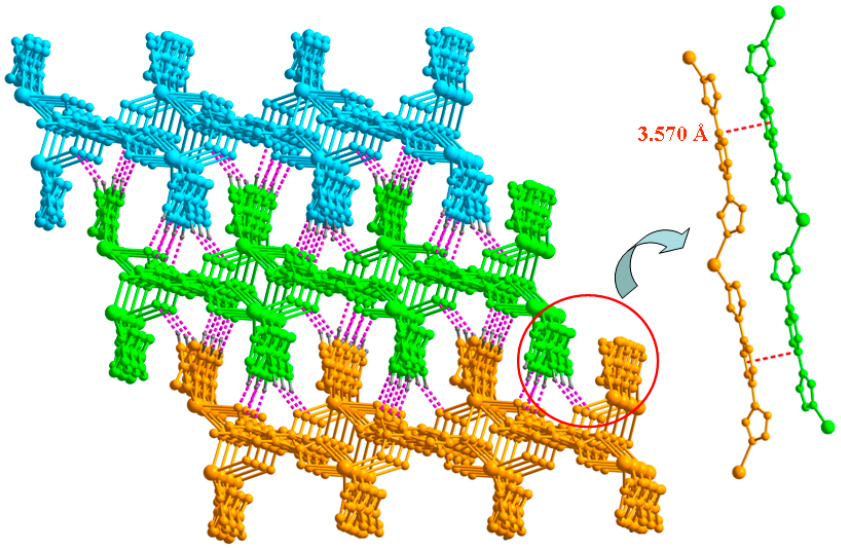

Figure 5. 3D structure of **1** extended by weak hydrogen bonding and π-π stacking interactions.

Table 2. Selected bond lengths (Å) and bond angles (°) for **1**.

Bond	*d*	Bond	*d*
Cd(1)–N(1)	2.264(4)	Cd(1)–N(4) [i]	2.274(4)
Cd(1)–O(3) [ii]	2.340(3)	Cd(1)–O(1)	2.364(3)
Cd(1)–O(2)	2.424(4)	Cd(1)–N(5) [iii]	2.443(4)
Angle	**ω**	**Angle**	**ω**
N(1)–Cd(1)–N(4) [i]	100.72(15)	N(1)–Cd(1)–O(3) [ii]	81.50(13)
N(4) [i]–Cd(1)–O(3) [ii]	112.25(15)	N(1)–Cd(1)–O(1)	93.06(14)
N(4) [i]–Cd(1)–O(1)	148.56(15)	O(3) [ii]–Cd(1)–O(1)	97.58(12)
N(1)–Cd(1)–O(2)	98.50(15)	N(4) [i]–Cd(1)–O(2)	95.05(15)
O(3) [ii]–Cd(1)–O(2)	152.30(11)	O(1)–Cd(1)–O(2)	54.72(12)
N(1)–Cd(1)–N(5) [iii]	159.79(15)	N(4) [i]–Cd(1)–N(5) [iii]	93.36(15)
O(3) [ii]–Cd(1)–N(5) [iii]	79.77(13)	O(1)–Cd(1)–N(5) [iii]	82.00(14)
O(2)–Cd(1)–N(5) [iii]	94.59(14)		

Symmetry codes: [i] $x, y + 1, z$; [ii] $-x + 1/2, -y + 1/2, -z$; [iii] $x, -y + 1, z - 1/2$.

Table 3. Hydrogen bond lengths (Å) and bond angles (°) for **1**.

D–H···A	d(D–H)	d(H···A)	d(D···A)	∠DHA
N(2)–H(2A)···O(4) [a]	0.8600	1.9700	2.816(6)	169.00
N(3)–H(3)···O(3) [b]	0.8600	2.0800	2.806(6)	142.00
N(5)–H(5B)···O(4) [c]	0.9000	2.0900	2.830(5)	138.00
C(11)–H(11)···O(1) [d]	0.9300	2.4200	3.351(8)	174.00
C(12)–H(12)···O(2) [a]	0.9300	2.5000	3.406(7)	166.00
C(13)–H(13)···O(3) [c]	0.9300	2.4800	3.277(5)	144.00

Symmetry codes: [a] $1 - x, y, 1/2 - z$; [b] $1/2 + x, -1/2 + y, z$; [c] $1/2 - x, 1/2 + y, 1/2 - z$; [d] $1/2 - x, 1/2 - y, -z$.

3.2. Thermal Analysis and Powder X-ray Diffraction Analysis

The thermal stability of the framework was investigated by thermogravimetric analysis (TGA) in the N_2 atmosphere from 20–700 °C. As shown in Figure 6, no weight losses were observed for complex **1**, until the framework collapse at about 380 °C, which was well consistent with the crystal structural composition of **1**. The phase purity of the bulk sample of **1** can be confirmed by the powder XRD experiment. As shown from Figure 7, the phase purity of the sample could be proven because the experimental pattern of the as-synthesized sample was consistent with the simulated one.

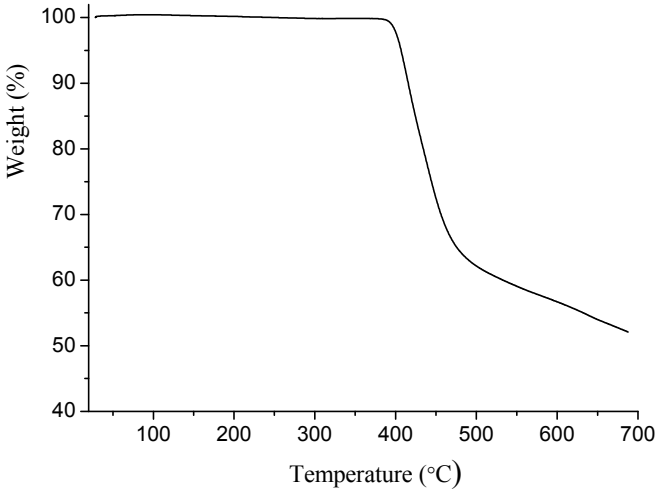

Figure 6. Thermal analysis curve of complex **1**.

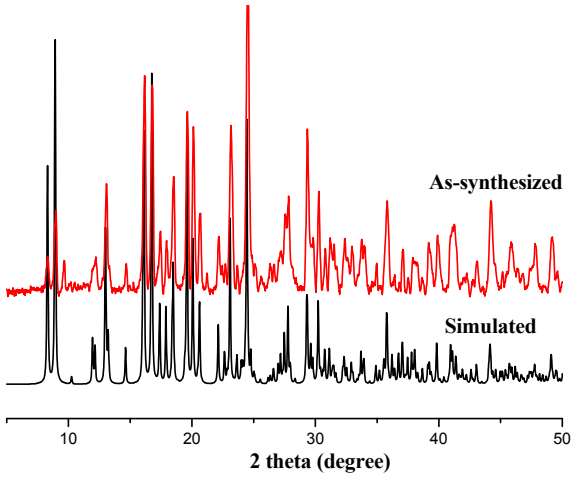

Figure 7. Simulated and experimental power X-ray diffraction (XRPD) pattern of complex **1**.

3.3. Diffuse Reflectance Spectra

The solid state optical diffuse reflection spectra at room temperature were investigated for complex **1** (Figure 8). The compound showed absorption peaks at 305 nm, which is attributable to the $\pi \rightarrow \pi^*$ transition of the conjugated organic ligand [26]. In order to study the semiconductivity of the complexes, the diffuse reflectance data were measured and transformed into a Kubelka–Munk function to obtain their band gaps (Eg). The band gap Eg of compound **1** can be determined based on the theory of optical absorption for the direct band gap semiconductor: $(Ah\nu)^2 = B(h\nu - Eg)$, where B is a constant corresponding to the material itself [26]. As shown in Figure 9, the optical band gap of complex **1** obtained by extrapolation of the linear portion of the diffuse reflectance spectra are estimated as approximately 3.12 eV, which exhibits the nature of semiconductivity, indicating that the compound is optical semiconductor [27].

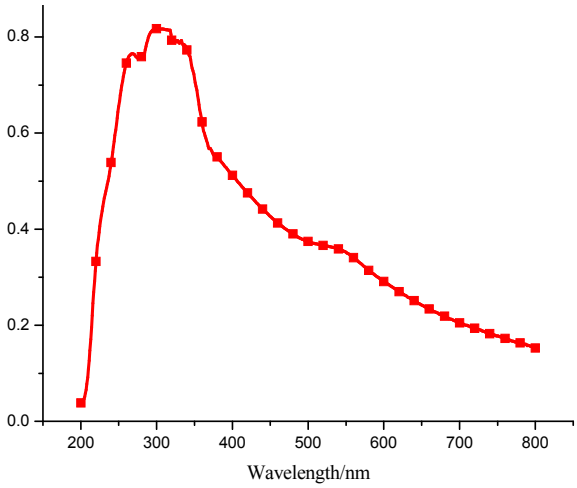

Figure 8. The solid-state diffuse reflectance UV-Vis spectra for the complex.

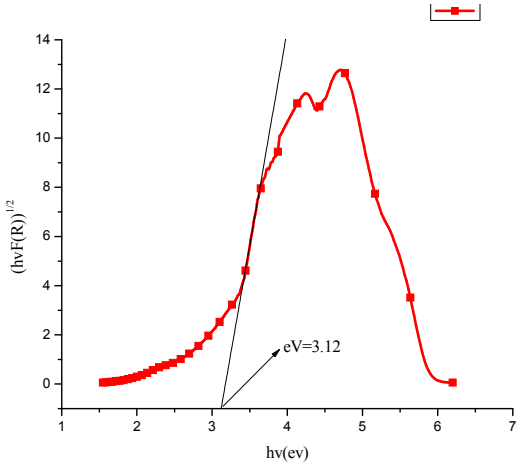

Figure 9. The band gap with 3.12 ev by the treatment with the Kubelka–Munk function.

3.4. Photoluminescent Property

Luminescent CPs, especially consisting of the d^{10} closed-shell metal center and π-conjugated organic ligand system, have been proved to have the ability to adjust the emission because of their interaction between metal and ligands [28,29]. Therefore, we carry out the solid-state photoluminescent property of complex **1**, and the organic ligands are depicted in Figure 10. The complex **1** shows strong broad photoluminescence emission at 435 nm upon excitation at 359 nm. The intense emission band at 455 nm was observed for a free H_2L ligand upon excitation at 342 nm, which may be ascribed to $\pi^* \rightarrow \pi$ transition because the conjugative effect of H_2L ligand [30]. However, the H_2nobda ligand shows weak emission maxima at 420 nm upon excitation at 338 nm, much lower than that of the π-conjugated H_2L ligand, because the fluorescent emission of the $\pi^* \rightarrow$ n transition resulting from benzene-dicarboxylate ligands could nearly be neglected in comparison with that arising from the $\pi^* \rightarrow \pi$ transition of the π-conjugated H_2L ligand. Therefore, benzene-carboxylate ligands made almost no contribution to the fluorescent emission of supermolecular polymer [31,32]. In this compound, the emission bands of complex **1** is 20 nm blue-shifted, and it shows intensive emission in comparison to the free H_2L ligand (Figure 11), which may be the intraligand fluorescence, since the free ligand exhibited a similar emission under the same condition [33,34].

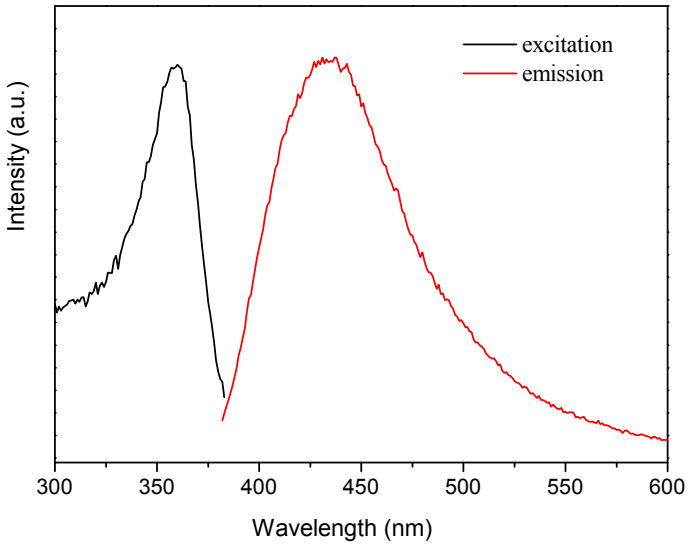

Figure 10. Solid-state photoluminescent spectra of **1** at room temperature.

Figure 11. The photographic picture exposed at 365 nm under an ultraviolet lamp (H_2L ligand, (**left**); complex **1**, (**right**)).

Furthermore, we carried out the study of the corresponding quantum yield (QY) and decay lifetimes for complex **1**. The QY value of compound **1** is 0.86% (Figure 12). In addition, the luminescence lifetime of complex **1** is 81.25 ns (Figure 13), that luminescence decay curves was fitted by exponential function as $I(t) = A \exp(-t/\tau)$. Therefore, the emissions of **1** should arise from a singlet state, because the luminescence lifetime is much shorter than the ones resulting from a triplet state ($>10^{-3}$ s) [35].

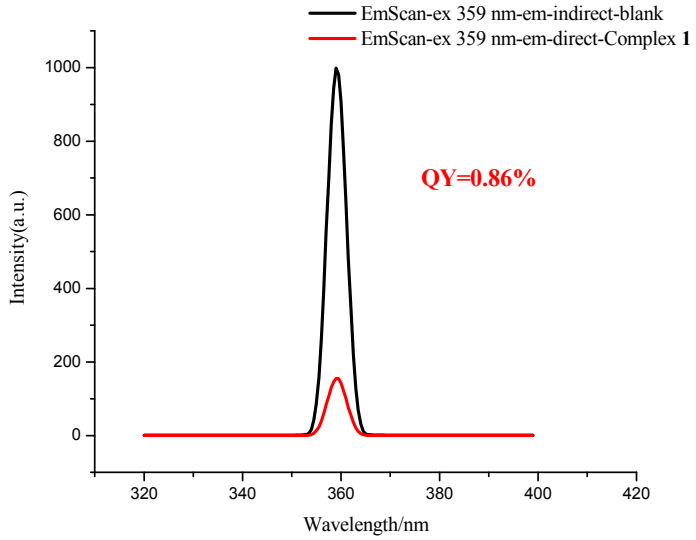

Figure 12. The QY curves of complex **1**.

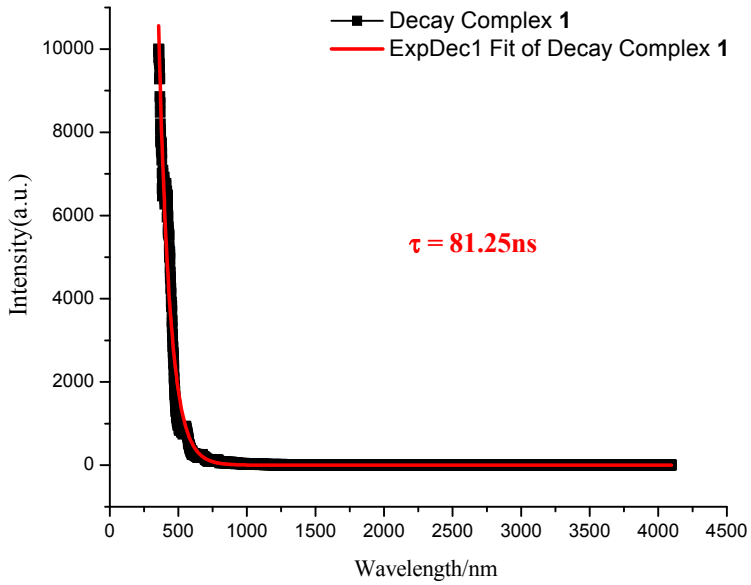

Figure 13. Luminescence decay curve for compound **1** (the black and red lines represent experimental data and fitting result, respectively).

4. Conclusions

In summary, a new coordination polymer $[Cd(H_2L)(nobda)]_n$ has been successfully synthesized by the reaction of the mixed N-donor imidazole and O-donor carboxylate ligands with $Cd(NO_3)_2{\cdot}4H_2O$. The carboxy groups from H_2nobda were completely deprotonated to $nobda^{2-}$ anions, linking the Cd(II) atoms into an infinite 2D layer structure. Furthermore, classic weak hydrogen bond and $\pi-\pi$ stacking interactions further connected the adjacent 2D layers, forming a 3D supermolecular structure. Compound **1** exhibits an emission band at 435 nm upon excitation at 359 nm. Moreover, the study of the corresponding quantum yield and decay lifetimes of **1** were also performed.

Author Contributions: M.-A.Z. and S.-S.H. synthesized the ligand H_2L. F.D. synthesized complex **1**. J.-L.L. carried out the analysis and S.-S.C. guided the manuscript.

Funding: Natural Science Foundation of Colleges of Anhui Province (KJ2017ZD29); Fuyang Government and Fuyang Normal University (XDHX201707).

Acknowledgments: This project was supported by the Natural Science Foundation of Colleges of Anhui Province (KJ2017ZD29) and the cooperative project of the Fuyang Government and Fuyang Normal University (XDHX201707).

Conflicts of Interest: The authors declare no conflict of interest.

References

1. Yuan, S.; Zhang, P.; Zhang, L.; Garcia-Esparza, A.T.; Sokaras, D.; Qin, J.S.; Feng, L.; Day, G.S.; Chen, W.; Drake, H.F.; et al. Exposed equatorial positions of metal centers via sequential ligand elimination and installation in MOFs. *J. Am. Chem. Soc.* **2018**, *140*, 10814–10819. [CrossRef] [PubMed]
2. Flaig, R.W.; Osborn Popp, T.M.; Fracaroli, A.M.; Kapustin, E.A.; Kalmutzki, M.J.; Altamimi, R.M.; Fathieh, F.; Reimer, J.A.; Yaghi, O.M. The chemistry of CO_2 capture in an amine-functionalized metal−organic framework under dry and humid conditions. *J. Am. Chem. Soc.* **2017**, *139*, 12125–12128. [CrossRef] [PubMed]
3. Zhao, D.; Liu, X.H.; Guo, J.H.; Xu, H.J.; Zhao, Y.; Lu, Y.; Sun, W.Y. Porous metal–organic frameworks with chelating multiamine sites for selective adsorption and chemical conversion of carbon dioxide. *Inorg. Chem.* **2018**, *57*, 2695–2704. [CrossRef] [PubMed]
4. Cui, Y.; Yue, Y.; Qian, G.; Chen, B. Luminescent functional metal-organic frameworks. *Chem. Rev.* **2012**, *112*, 1126–1162. [CrossRef] [PubMed]
5. Rowland, C.A.; Lorzing, G.R.; Gosselin, E.J.; Trump, B.A.; Yap, G.P.A.; Brown, C.M.; Bloch, E.D. Methane storage in paddlewheel-based porous coordination cages. *J. Am. Chem. Soc.* **2018**, *140*, 11153–11157. [CrossRef] [PubMed]
6. Kreno, L.E.; Leong, K.; Farha, O.K.; Allendorf, M.; Van Duyne, R.P.; Hupp, J.T. Metal_organic framework materials as chemical sensors. *Chem. Rev.* **2012**, *112*, 1105–1125. [CrossRef] [PubMed]
7. Yoon, M.; Srirambalaji, R.; Kim, K. Homochiral Metal_organic frameworks for asymmetric heterogeneous catalysis. *Chem. Rev.* **2012**, *112*, 1196–1231. [CrossRef] [PubMed]
8. Zhao, D.; Liu, X.H.; Zhu, C.D.; Kang, Y.S.; Wang, P.; Shi, Z.Z.; Lu, Y.; Sun, W.Y. Efficient and reusable metal-organic framework catalysts for carboxylative cyclization of propargylamines with carbon dioxide. *ChemCatChem* **2017**, *9*, 4598–4606. [CrossRef]
9. Fan, L.; Kang, Z.; Shen, Y.; Wang, S.; Zhao, H.; Sun, H.; Hu, X.; Sun, H.; Wang, R.; Sun, D. Mixed matrix membranes based on metal−organic frameworks with tunable pore size for CO_2 separation. *Cryst. Growth Des.* **2018**, *18*, 4365–4371. [CrossRef]
10. Yao, Z.Q.; Li, G.Y.; Xu, J.; Hu, T.L.; Bu, X.H. A water-stable luminescent Zn^{II} metal-organic framework as chemosensor for high-efficiency detection of CrVI-anions ($Cr_2O_7^{2-}$ and CrO_4^{2-}) in aqueous solution. *Chem. Eur. J.* **2018**, *24*, 3192–3198. [CrossRef] [PubMed]
11. Furukawa, H.; Cordova, K.E.; O'Keeffe, M.; Yaghi, O.M. The chemistry and applications of metal-organic frameworks. *Science* **2013**, *341*, 1230444. [CrossRef] [PubMed]
12. Li, J.R.; Zhou, H.C. Bridging-ligand-substitution strategy for the preparation of metal–organic polyhedra. *Nat. Chem.* **2010**, *2*, 893–898. [CrossRef] [PubMed]

13. Jiang, M.; Li, B.; Cui, X.; Yang, Q.; Bao, Z.; Yang, Y.; Wu, H.; Zhou, W.; Chen, B.; Xing, H. Controlling pore shape and size of interpenetrated anion-pillared ultramicroporous materials enables molecular sieving of CO2 combined with ultrahigh uptake capacity. *ACS Appl. Mater. Interfaces* **2018**, *10*, 16628–16635. [CrossRef] [PubMed]
14. Li, X.Y.; Ma, L.N.; Liu, Y.; Hou, L.; Wang, Y.Y.; Zhu, Z. Honeycomb metal–organic framework with lewis acidic and basic bifunctional sites: Selective adsorption and CO_2 catalytic fixation. *ACS Appl. Mater. Interfaces* **2018**, *10*, 10965–10973. [CrossRef] [PubMed]
15. Lysenko, A.B.; Bondar, O.A.; Senchyk, G.A.; Rusanov, E.B.; Srebro-Hooper, M.; Hooper, J.; Prsa, K.; Krämer, K.W.; Decurtins, S.; Waldmann, O.; et al. On the border between low-nuclearity and one-dimensional solids: A unique interplay of 1,2,4-triazolyl-based $\{Cu^{II}_5(OH)_2\}$ clusters and MoVI-oxide datrix. *Inorg. Chem.* **2018**, *57*, 6076–6083. [CrossRef] [PubMed]
16. Zhang, Z.Y.; Xiao, L.; Chen, S.S.; Qiao, R.; Yang, S. A novel Zn(II) complex with 4-connected umc topology: Synthesis, crystal structure and luminescent property. *Chin. J. Struct. Chem.* **2017**, *36*, 819–824.
17. Xiong, J.; Wang, K.; Yao, Z.; Zou, B.; Xu, J.; Bu, X.H. Multi-stimuli responsive fluorescence switching from a pyridine functionalized tetraphenylethene AIEgen. *ACS Appl. Mater. Interfaces* **2018**, *10*, 5819–5827. [CrossRef] [PubMed]
18. Chen, S.S.; Chen, M.; Takamizawa, S.; Chen, M.S.; Su, Z.; Sun, W.Y. Temperature dependent selective gas sorption of the microporous metal-imidazolate framework [Cu(L)] [H_2L = 1,4-di(1H-imidazol-4-yl) benzene]. *Chem. Commun.* **2011**, *47*, 752–754. [CrossRef] [PubMed]
19. Chen, S.S.; Chen, M.; Takamizawa, S.; Wang, P.; Lv, G.C.; Sun, W.Y. Porous cobalt(II)-imidazolate supramolecular isomeric frameworks with selective gas sorption property. *Chem. Commun.* **2011**, *47*, 4902–4904. [CrossRef] [PubMed]
20. Chen, S.S.; Sheng, L.Q.; Zhao, Y.; Liu, Z.D.; Qiao, R.; Yang, S. Syntheses, structures, and properties of a series of polyazaheteroaromatic core-based Zn(II) coordination polymers together with carboxylate auxiliary ligands. *Cryst. Growth Des.* **2016**, *16*, 229–241. [CrossRef]
21. Chen, S.S.; Qiao, R.; Sheng, L.Q.; Zhao, Y.; Yang, S.; Chen, M.M.; Liu, Z.D.; Wang, D.H. Cadmium(II) and zinc(II) complexes with rigid 1-(1*H*-imidazol-4-yl)-3-(4*H*-tetrazol-5-yl)benzene and varied carboxylate ligands. *CrystEngComm* **2013**, *15*, 5713–5725. [CrossRef]
22. Zhu, M.A.; Guo, X.Z.; Chen, S.S. Synthesis, crystal structure and luminescent property of a Zn(II) complex based on 4-imidazole-carboxylate ligand. *Chin. J. Struct. Chem.* **2017**, *36*, 1348–1354.
23. Sheldrick, G.M. A short history of SHELX. *Acta Cryst. A* **2008**, *64*, 112–122. [CrossRef] [PubMed]
24. Blatov, V.A. *TOPOS, A Multipurpose Crystallochemical Analysis with the Program Package*; Samara State University: Samara, Russia, 2009.
25. Gu, Y.F.; Liu, X.T.; Zhang, Y.; Zhang, S.M.; Chang, Z.; Bu, X.H. Supramolecular recognition of benzene homologues in a 2D coordination polymer through variable inter-layer π–π interaction. *CrystEngComm* **2018**, *20*, 3313–3317. [CrossRef]
26. Yang, Y.J.; Wang, M.J.; Zhang, K.L. A novel photoluminescent Cd(II)–organic framework exhibiting rapid and efficient multi-responsive fluorescence sensing for trace amounts of Fe^{3+} ions and some NACs, especially for 4-nitroaniline and 2-methyl-4-nitroaniline. *J. Mater. Chem. C* **2016**, *4*, 11404–11418. [CrossRef]
27. Su, J.; Yao, L.; Zhao, M.; Wang, H.; Zhang, Q.; Cheng, L.; Tian, Y. Structural induction effect of a zwitterion pyridiniumolate for metal–organic frameworks. *Inorg. Chem.* **2015**, *54*, 6169–6175. [CrossRef] [PubMed]
28. Wang, Z.J.; Han, L.J.; Gao, X.J.; Zheng, H.G. Three Cd(II) MOFs with different functional groups: Selective CO_2 sapture and metal ions detection. *Inorg. Chem.* **2018**, *57*, 5232–5239. [CrossRef] [PubMed]
29. Xu, J.; Bai, Z.S.; Chen, M.S.; Su, Z.; Chen, S.S.; Sun, W.Y. Metal–organic frameworks with six- and four-fold interpenetration and their photoluminescence and adsorption property. *CrystEngComm* **2009**, *11*, 2728–2733. [CrossRef]
30. Shi, Z.; Pan, Z.; Jia, H.; Chen, S.; Qin, L.; Zheng, H. Zn(II)/Cd(II) terephthalate coordination polymers incorporating bi-, tri-, and tetratopic phenylamine derivatives: Crystal structures and photoluminescent properties. *Cryst. Growth Des.* **2016**, *16*, 2747–2755. [CrossRef]
31. Hua, J.A.; Zhao, Y.; Liu, Q.; Zhao, D.; Chen, K.; Sun, W.Y. Zinc(II) coordination polymers with substituted benzenedicarboxylate and tripodal imidazole ligands: Syntheses, structures and properties. *CrystEngComm* **2014**, *16*, 7536–7546. [CrossRef]

32. Li, Y.W.; Ma, H.; Chen, Y.Q.; He, K.H.; Li, Z.X.; Bu, X.H. Structure modulation in Zn(II)–1,4-bis(imidazol-1-yl) benzene frameworks by varying dicarboxylate anions. *Cryst. Growth Des.* **2012**, *12*, 189–196. [CrossRef]
33. Su, S.Q.; Qin, C.; Guo, Z.Y.; Guo, H.D.; Song, S.Y.; Deng, R.P.; Cao, F.; Wang, S.; Li, G.H.; Zhang, H.J. Five three/two-fold interpenetrating architectures from self-assembly of fluorene-2,7-dicarboxylic acid derivatives and d^{10}metals. *CrystEngComm* **2011**, *13*, 2935–2941. [CrossRef]
34. Li, X.J.; Jiang, F.L.; Wu, M.Y.; Chen, L.; Qian, J.J.; Zhou, K.; Yuan, D.Q.; Hong, M.C. Construction of two microporous metal–organic frameworks with flu and pyr topologies based on $Zn_4(\mu_3\text{-}OH)_2(CO_2)_6$ and $Zn_6(\mu_6\text{-}O)(CO_2)_6$ secondary building units. *Inorg. Chem.* **2014**, *53*, 1032–1038. [CrossRef] [PubMed]
35. Yang, D.L.; Zhang, X.; Yao, Y.G.; Zhang, J. Structure versatility of coordination polymers constructed from a semirigid ligand and polynuclear metal clusters. *CrystEngComm* **2014**, *16*, 8047–8057. [CrossRef]

© 2018 by the authors. Licensee MDPI, Basel, Switzerland. This article is an open access article distributed under the terms and conditions of the Creative Commons Attribution (CC BY) license (http://creativecommons.org/licenses/by/4.0/).